Slip rate of the Düzce segment of the North Anatolian Fault Zone from offset geomorphic markers

S. Pucci [1 and 2] *, P.M. De Martini [1] and D. Pantosti [1]

[1] Sismologia e Tettonofisica, Istituto Nazionale di Geofisica e Vulcanologia, via di Vigna Murata, 605, 00143 Roma, Italy

[2] Dipartimento di Scienze della Terra, Universita' degli Studi di Perugia, piazza dell'Università, 06128 Perugia, Italy

*Corresponding Author, pucci@ingv.it

Keywords: tectonic geomorphology, geomorphic markers, slip rate, strike-slip, 1999 Düzce earthquake.

Abstract

We provide new estimates on the Quaternary slip rate of the active transform margin of North Anatolia.

We investigated the area struck by 12 November 1999, Mw 7.1 earthquake, that ruptured the Düzce fault segment. In order to analyze the spectacular tectonically driven cumulative landforms and the drainage pattern settings, we carried out a 1:25 000-scale geological and geomorphological map along the fault trace. We reconstruct and describe, as offset geomorphic markers, right-hand stream deflections and remnant of an old alluvial fan modeled by fluvial terraces. The streams are deflected for a total of about 100 m and the onset of the offset was radiocarbon dated about 7000 yr BP. The two documented and correlated Late Pleistocene, terrace risers are offset of about 300 and 890 m, respectively. These terrace risers were dated by means of Optically Stimulated Luminescence (OSL) method about 21 000 yr BP and 60 000 yr BP. These ages and offsets translate to a constant rate of deformation of the Düzce Fault, at different time scales, of 14.0 ± 1.8 mm/yr and disproves a time-variable model at least for the last 60 000 yr.

Considering the GPS-measured strain accumulation due to the plate motion along this part of the North Anatolian Fault Zone, the Düzce Fault importantly participates to the North Anatolian margin deformation, suggesting a present-day partitioning of displacement rates with the

Mudurnu fault to the south and assuming a relevant role in the seismic hazard of the area.

1. Introduction

The near-fault, geological slip-rate data, along with the far-field geodetic data, are the observational basis for physical models of the earthquake deformation cycle [Reid, 1910; Shimazaki and Nakata, 1980; Shwartz and Coppersmith, 1984; Wallace, 1987] and the assessment of seismic hazards. In regions where plate boundary zones are composed by systems of faults that concurrently accommodate the deformation on a broad area, the knowledge of slip rate magnitude and distribution is critical for: 1) determine how deformation is partitioned among the faults; 2) estimate the nature of the spatial and temporal fault interactions; 3) evaluate whether fault slip-rates are constant or time-variable, at different time scales; 4) reconstruct the plate boundary evolution.

Along the active transform margin of North Anatolia, the prominent geomorphic signature of strike slip faulting is one of the main direct consequences of the long-lasting (Late Miocene-Early Pliocene to present [Barka, 1992, Şengör et al., 2005] and important strain due to the extrusion of the Anatolian block (20-30 mm/yr by means of GPS data [Reilinger et al., 1997 and 2000; Straub et al., 1997; McClusky et al., 2000; Kahle et al., 1999 and 2000]; fig. 1). However, limited documented offset of structural or geomorphic markers exist along the 1500 km-long North Anatolian Fault Zone (NAFZ) [Dhont et al., 1998; Armijo et al., 1999; Hubert-Ferrari et al., 2002; Polonia et al., 2004; Şengör et al., 2005] and thus the geological strain rate is poorly constrained (fig. 2). This highlights that there is still need for

detailed case studies on slip rates to fill in knowledge of the NAFZ activity in time and space.

With this aim, we investigated the area struck by 12 November 1999, Mw 7.1 earthquake, that ruptured the Düzce segments, where the NAFZ splits in two main fault strands. The Düzce fault is a natural laboratory where both spectacular 1999 surface ruptures and impressive tectonically driven landforms are present and can be studied in order to derive Quaternary slip rate estimates. This area is particularly favorable because of (1) extensive presence of faulted Pleistocene and Holocene continental deposits, (2) high preservation potential of the landforms with respect to the time scale of the tectonic process, and (3) deformation appears to be recorded and localized in the landscape close to the surface expression of the fault (Pucci et al., 2006a and 2006b).

In this work we present cumulative fault-related deformation and offset geomorphic markers, that should be intended as an enrichment of the data-set of slip rate estimates over various time periods for the NAFZ.

We carried out a 1:25 000-scale geological and geomorphological mapping along the fault trace. The observations were made on 1:18 000 and 1:35 000 scale aerial photographs, 20-m-resolution Digital Elevation Model (interpolated from 1:25 000-scale topography, 10 m digital contours), and standard morphometric derivatives (hill-shaded and slope angle maps), all supported by field survey.

In the following, after a brief introduction of the tectonic framework of the NAFZ and of the Düzce fault segment, we describe offset geomorphic markers and their dating and in particular: (1) right-hand stream deflections and their alluvial terraces; (2) remnant of an old alluvial fan modeled by

fluvial terraces. In order to understand whether changes in the fault motion occurred in space and time, we discuss the comparison at different time-scale of the obtained slip rates.

2. Overview on the North Anatolian Fault Zone (NAFZ)

The NAFZ is an active right-lateral system, about 1500 km long, which bounds to the north the westward-extruding Anatolian block [McKenzie, 1972; Şengör, 1979; Barka, 1992; Şaroğlu et al., 1992] (fig. 1) that, based on the age of fault-related basins deposits, is supposed to be active since Late Miocene [Şengör et al., 1985; Dewey et al., 1986; Şengör et al., 2005] or Early Pliocene [Barka, 1992]. This transform margin mainly follows a pre-existing zone of weakness, the Izmir-Ankara-Erzincan suture zone, inherited from Late Cretaceous-Early Miocene collisional phase [Sengör and Yılmaz, 1981; Şengör et al., 1985; Okay, 1989; Yilmaz and Yilmaz, 2004]. To the east of the town of Bolu (figs. 1 and 2), the NAFZ is formed by a main single trace but, west of it, it splays into two main strands, the Düzce and the Mudurnu fault segments. Farther west, it splays again into three major strands and most of the present-day strain is considered to be accommodated along the northernmost one [Barka and Kadinski-Cade, 1988; Straub et al., 1997], that forms the pull-apart basins hosting the Marmara Sea [Wong et al., 1995; Le Pichon et al., 2001; Armijo et al., 1999; Okay et al., 1999].

Seismicity along the NAFZ is characterized by frequent moderate to large earthquakes (M>7) with focal mechanisms solutions that show

essentially pure right-lateral strike-slip motion [Canitez and Ucer, 1967; McKenzie, 1972; Reinecker et al., 2004, see http://www.world-stress-map.org]. The number of large historical earthquakes attributed to the NAFZ places this fault among the most active strike-slip structures worldwide [Ambraseys, 1970; Ambraseys and Finkel, 1995; Ambraseys, 2002] and testifies that the present-day high deformation rate is seismically accommodated with rates of 20 ± 10 mm/yr (from seismic moment release over the past 100-400 years [Jackson and McKenzie, 1988; Westaway, 1994]).

Regional GPS networks measured present-day strain-rates in the northern part of the Anatolian block up to ca. 25 ± 5 mm/yr [Reilinger et al., 1997 and 2000; Straub et al., 1997; McClusky et al., 2000; Kahle et al., 1999 and 2000] and show vectors that are oriented WNW in the easternmost region, E-W in the centre and SW in the Aegean (fig. 1).

Limited documented geological slip-rates indicate the NAFZ slip rates with a large variability over various timescale, from 2 mm/yr up to 52 mm/yr (fig. 2). These values are much lower or present larger uncertainties than the present-day geodetic measurements, suggesting an acceleration of the deformation over time or a limitation in measuring and dating geological offsets. According to some Authors the NAFZ presents a uniform amount of deformation all along the fault and has accumulated a total geologic displacement of 85 ± 15 km [Hubert-Ferrari et al., 2002] or of 75 ± 10 km [Westaway, 1994 and Armijo et al., 1999]. Conversely, according to Barka [1992], since the Early Pliocene, the NAFZ has accumulated a total geologic displacement of 40 ± 5 km, with decrease to 25 ± 5 km east of the Marmara Sea. Therefore, on the basis of the NAFZ age, the total displacements

translate to geological slip rate ranging from 6.0 up to 23 mm/yr (1, 10 and 11 in fig. 2).

The punctual long-term (i.e. Plio-Pleistocene) and short-term (i.e. Holocene) slip rates show a high variability. These are reported in figure 2 and are: 7 up to 23 mm/y [Erinc, 1953; Gaudemer et al., 1989; Barka and Gulen, 1989; Huber-Ferrari et al., 2002; Şengör et al., 2005] from deflected Early Pliocene river system (6-9 and 12-13 in fig. 2); 10.3 ± 8.2 mm/yr from a Pliocene-Middle Pleistocene offset basin (4 in fig. 2) [Dhont et al., 1998]; 10 ± 1.5 mm/yr from a 10,200 yr old underwater stream deflection (2 in fig. 2) [Polonia et al., 2004]; 18.4 ± 2.6 mm/yr and 17.8 ± 5.3 mm/yr from 10,000-12,000 yr old and 1600-4000 yr old stream terrace offsets, respectively (4 and 6 in fig. 2) [Hubert-Ferrari et al., 2002].

The data collected suggest that the rate of motion of NAFZ has being changing both in time and space during its history from 6.0 mm/yr to 20-30 mm/yr. Yet, the scientific community proposes two different reasons for this: 1) Armijo et al. [1999] and Hubert-Ferrari et al. [2002] accepts as true the Pliocene age of the western part of the NAFZ and hypothesizes a westward propagation of the fault, starting from its Late Miocene easternmost part [Hubert-Ferrari et al., 2003], and interpret the western, higher short-term slip rates as due to a recovery strain; 2) Şengör et al. [2005] consider all the North Anatolian transform margin coeval (13-11 Ma old), but, starting from a partitioned and wider deformation zone; the deformation becoming localized (along the present NAFZ) at different times along its strike. Under this light, the transform margin presents a diachronic acceleration of the slip rate, slower to the west with respect to the east.

2.1 The Düzce fault segment of the NAFZ

The Düzce fault segment has an average E-W trend and a clear geomorphic expression for about 40 km. It separates the Paleozoic-Eocene formations of the Almacik block from the Quaternary continental deposits of the Pliocene Düzce basin (fig. 3). The Düzce Basin contains a 260m-thick alluvial-lacustrine deposits that sits mainly on Eocene volcanogenic flysch [Komut, 2005]. The basin infill is formed by Late Pleistocene-Holocene, Gilbert deltas sediments that overlie unconformably Pliocene-Early Pleistocene sequence [Emre et al., 1998]. Although with internal differences, the overall long-term morphological expression of the Düzce fault depicts a single and continue structural element that produces uplift of the range, to the south, with respect to the plain, to the north.

As already mentioned, in this part of the North Anatolian Fault, the Düzce fault to the north and the Mudurnu fault to the south represent the two main strands (fig. 3). According to Ayhan et al. [1999 and 2001], the Düzce Fault accommodates 33% to 50% (i.e. up to 10 mm/yr) of the present-day GPS strain of the NAFZ. Geological slip rates obtained from the analysis of offset geomorphic markers of the Düzce and the Mudurnu faults are not known. Conversely, some slip rates are derived from paleoseismological studies are of 13.5 ± 4.5 mm/yr for the Düzce fault [Pantosti et al., submitted] and 11 ± 5 mm/yr for the Mudurnu fault [Ikeda et al., 1991; Yoshioka et al., 1991; Palyvos et al., submitted].

The most recent coseismic rupture along the Düzce Fault occurred on 12 November 1999 (Mw 7.1, USGS, KOERI), producing right-lateral

surface faulting for a total length of ca. 40 km and a mean dextral offset of 2.7 m [Akyuz et al., 2000 and 2002; Pucci et al., 2006b]. The focal mechanism solution of the Düzce earthquake shows almost pure, E-W trending, dextral strike-slip movement, with a slight normal component (fig. 3). The coseismic ruptures do not exactly run at the mountain-piedmont interface, but affect both basin infill deposits and bedrock with a slightly northward-convex trajectory.

3. The Düzce fault landforms

We carried out geomorphic analysis along the 1999 rupture zone (hereinafter referred as near-fault analysis). Particular attention has been devoted to the drainage pattern analysis and to the setting of depositional and tectonic landforms, as well as to the recognition of recent continental deposits, crucial in order to detect suitable sediments for dating. The 1:25,000-scale geological and geomorphological map of the Düzce Fault (fig. 5) shows landforms, related to the erosional and the depositional processes that have been shaping the Almacik range-front, strongly coupled with near-fault tectonic landforms related to fault location and activity.

The erosion of the Almacik block provided important sediment production for the Düzce Basin. These sediments that cover the foot of the range-front are mainly alluvial fans that merge into coalescent aprons (hereinafter referred as bajadas) composed of Middle-Late Pleistocene alluvial fan and Late Pliocene-Early Pleistocene conglomerate-sandstone units (zone x, fig. 5) [Herece and Akay, 2003], and also of active Holocene

fans, deposited in subsequent incisions of the old bajadas (spot y, fig. 5). These generally loose and soft recent deposits recorded persistent landform modification due to faulting and developed well-expressed tectonic-related morphologies whose topography controlled the drainage pattern. Such features are clearly not related to the dynamics of the bajada, since they present tectonic deformations of the original depositional layers (fig. 6). The most common tectonic landforms in the study area are: tilted surfaces, fault escarpments, benches, saddles alignments, linear valleys, shutter ridges, pressure ridges, and sag ponds (fig. 5). This tectonic landforms appear to be the surface expression of a localized slip plane at depth, and the width of the near-fault deformation zones at the surface is related both to the thickness of young alluvial cover sequences and to free surface effects, as observed along other seismogenic structures (e.g. Landers [Sieh et al., 1993; Jhonson et al., 1994; Lazarte et al., 1994]; Dast-e Bayaz [Tchalenko and Ambraseys, 1970; Tchalenko and Barberian 1975]). Such tectonic landforms reflect also a small vertical component of deformation, resulting from strike-slip movement along a non rectilinear fault plane that produces transtension at releasing bends (e.g. spots z, fig. 5a) and transpression at restraining bends (e.g. spots q, fig. 5).

Along the western section of the Düzce fault, the 1999 coseismic fault trace bounds the triangular embayments of the range front, that host bajadas. As already mentioned, the rupture follows a saw-tooth trajectory (e.g. spots k, fig. 5a) with a few E-W trending elements (e.g. spots w in fig. 5a), associated to subtle and youthful landforms suggesting they have hosted only a small cumulative deformation that may represent an incipient stage of evolution of the fault system from irregular to linear geometry [Pucci et al.,

2006a and 2006b]. Because the bajada of this section is bounded by the fault to the north, it has a topographic profile with steep fanheads and is characterized by linear and abrupt transitions to the alluvial-lacustrine deposits of the Düzce plain. Linear escarpments, with strong stream incisions across the bajada and suspended terraces can be found at the stream outlets along the range-front foot (spots h, fig. 5a), suggesting an important subsidence north of the Düzce Fault.

Conversely, the eastern section of the Düzce Fault (fig. 5b) presents a more regular, localized, prominent E-W trace parallel to the mean trend of the whole Düzce fault. This E-W trending section crosscuts both recent continental deposits and bedrock and is associated with well developed landforms indicating its persistent long-term activity. It is characterized by shutter and pressure ridges, 300 to 1000 m-long, up to 120 m high (e.g. spots r, fig. 5b), with elongated shapes and long axes paralleling the escarpment elements they are associated with. In many cases, the ridges act as natural dams for northward flowing drainages, being thus responsible for the formation of ponds and the trapping of Holocene fans against the scarp (e.g. spots t, fig. 5b). Only the easternmost part of this E-W trending section shows subtle near-fault tectonic landforms, going through the Holocene deposits of the Kaynasli pull-apart basin.

Overall, the 1999 displacement zone closely mimics the long-term tectono-morphologic pattern, since the coseismic vertical component of displacement emphasizes the pre-existing relief [see also Pucci et al., 2006a]. Geometry, location and style of the coseismic ruptures, strongly indicate that they have been persistent a long time (at least for several

seismic cycles), particularly along the eastern section of the Düzce Fault, where the deformation appears more localized.

4. The geomorphic markers

The pattern of streams in a such tectonically active regions contains important clues to understand fault movement and its interaction with stream development [Huang, 1993; Jackson et al., 1996]. The lateral displacement of a stream may result from active strike-slip faulting [Wallace, 1968] and the size and characteristics of its features, combined with age control at several locations, can be used to estimate the rate of fault displacement [e.g., Matsuda, 1967; Keller et al., 1982; Sieh and Jahns, 1984].

Streams of intermediate stream power have a great ability to keep the channels entrenched, and therefore directly controlled by the fault displacement, for a long time. The confinement in valleys apparently allow these channels to keep and accumulate their offset for a much longer time than the young gullies [Ouchi, 2004 and 2005]. On the other hand, old streams with large stream power have the ability to compete with each coseismic displacement, adjusting their watercourse and removing any evidence for short-term tectonic deformation. Only the features that are not more related to the present dynamic of these streams (e.g. flight of abandoned fluvial terraces), if preserved, can be interpreted as evidence for the ongoing deformation.

We found features that have been displaced and that provide a reference frame against which to gauge deformation, only along the

westernmost part of the east section of the Düzce Fault (fig. 4). We identified deflected drainage pattern at the Tilki-Cicubey area (area A in fig. 5b) and offset river terraces at the Beykoy-Degirmenbasi area (area B in fig. 5b). For these features, it was possible to hypothesize a probable initial undeformed geometry and to find recent deposits suitable for dating.

4.1 The Tilki-Cicubey area

The Tilki-Cicubey (A) area is associated with well-expressed, 400 to 800 m long, elongated tectonic ridges, along the base of the range front (e.g. spot x, fig. 7). Most of these ridges, ca. 70 m high with steep slopes, are made of a Paleozoic-Jurassic granitoid unit. The north-flowing drainages of this area show directions with high angles with respect to the strike of the Düzce Fault, which favor the preservation of anomalies [Allen, 1962]. These drainage system present similar right-hand stream deflections of about 100 m (e.g. spot y, fig. 7) and belongs to the same Strahler's [1952] order. Such deflections occurred because of the growth and offset of the ridges that acted as natural dams to their flow. Tectonic influence on drainage patterns along the fault is also expressed by stream piracy, since channels, clearly captured by beheaded and abandoned downstream reaches of adjacent larger channels, created apparent sinistral deflections (spot s in fig. 7 and fig. 8a) and perched ponding areas (spot p in fig. 7).

The measurement of the horizontal displacement is affected by several uncertainties [Ouchi, 2004 and 2005]. The fault offsets a stream by dragging along the fault line the downstream reach away from its upstream reach. In order to measure the net offset distance (D), we projected each stream reach onto the fault trace, on the basis of its direction. Because the deformation

zone of the fault crossing the offset channels is up to 10 m wide at the surface, the reach connecting the offset upstream and downstream reaches do not show a simple linear geometry and presents an angle (α) with the fault strike that is responsible of two possible measurements of the offset (Dl and Du in fig. 8b). Further uncertainty is introduced by the crossing angle between the two reaches and the fault (β) that is usually different for the upstream and the downstream reaches. In addition, the erosion due to the fluvial processes adds further uncertainties related to lithology, climate and interaction with tectonics.

4.1.1. Measuring the offset

In this area, we investigated in detail two locations with similar features: the Amcahasanbey (1, fig. 7)and the Cicubey sites (2, fig. 7).

The Amcahasanbey site shows the alignment of the bedrock shutter ridge with a 10 meter high ridge, made of alluvial deposits of an Holocene bajada remnant, that is characterized by an asymmetric profile (a flat surface and a gentle north-facing slope) (fig. 9), whose southern flank is bounded by a south-facing fault escarpment. In this site a stream flows north-eastward along an entrenched valley of the range front that, because of the south-facing fault escarpment, turns to the right to flows along the fault zone and after about hundred meters, cuts the natural dam through an outlet to the Düzce Basin (1, fig. 7 and 9). This stream tends to adjust its longitudinal profile, by the vertical component of each subsequent coseismic offset and by the shutter effect to the channel; this results in an upstream aggradation and a downstream degradation. In fact, when it flows along the south-facing fault escarpment the stream shows an aggradational behavior, discharging alluvial deposits and producing a ponded area (fig. 9). These morphologies

portray the recent stream history: first, we can assume that the river was free to flow and deposit along a quasi-straight channel (fig. 10a); then, it starts to incise both linear valleys and ridges and become entrenched, conceivably due to climatic changes; this impeded the stream to change its course (fig. 10b) and forced it to deflect following repeated movements of the fault (fig. 10c). During this second phase, the stream power was not enough to erode and oppose the tectonics and thus to straighten the stream course.

Following this reasoning to measure the accumulated strain, we projected on the fault trace the two parallel parts of the stream channel on the two fault blocks, and we tape measured in the field and on aerial photo the distance between them (spot x, fig. 10). This yields a stream deflection of 105 ± 25 m. Furthermore, the abrupt slope change between the aligned bedrock and Holocene ridges seems to have an erosional origin that suggests to be an abandoned left wall of the stream channel (spot w, fig 9a). Similarly, we projected and measured this abandoned left channel wall and the present one (spot y and w, respectively, fig 10), that yields a comparable deflection of 110 ± 10 m, that supports the stream deflection in being reliably tectonic-related.

The Cicubey site (2, fig. 7) presents analogy with the previous site. The Düzce Fault offset the upper and the lower reaches of the NNE-trending stream that is forced, by the south-facing fault escarpment, to turn sharply to the right. The stream deeply incises the 15 m-high ridge, that act as shutter (fig. 11). This landform is made of alluvial deposits, apparently belonging to the same Holocene bajada remnant found at the Amcahasanbey site. Along the south-facing fault escarpment the stream shows an aggradational cut-and-fill behavior, with discharged alluvial deposits and a young generation

of terraces. Here, taking in consideration the same assumptions and method of the previous case, we tape measured the present deflection of the stream channel, that yield 105 ± 25 m (fig. 11).

4.1.2. Dating

The estimate of the age of the Amcahasanbey (1) and Cicubey (2) paleosurfaces is based upon radiocarbon dating of buried organic material at sites shown in figure 10 and 11. In order to get the timing of the last depositional phase, prior to the stream entrenchment, that marks the onset of the stream deflection, the alluvial deposits of the Holocene bajada remnants were dated by C^{14}. Since an insufficient amount of charcoal or charred organic material was available for dating using conventional decay-counting methods, we dated the bulk organic matter. Samples were collected in a pit at 0.6-0.8 m below the surface. About 100 g of sampled material was sent to the Beta Analytic inc. laboratory for dating.

The sample were crushed, slurried and sieved prior to chemical pre-treatment and dating by decay counting (table 1). The bulk sediment samples provided a radiocarbon age of 5870 ± 50 yr BP, for the Amcahasanbey paleosurface (1) and 4150 ± 35 yr BP for the Cicubey paleosurface (2). These ages have been calibrated by means of the radiocarbon program CALIB REV5.0.1 (Copyright 1986-2005, M. Stuiver and P.J. Reimer [1993]), that provides 6720 ± 120 cal yr BP and 4670 ± 60 cal yr BP, respectively (2σ, table 1). On the basis of geomorphic considerations these surfaces where expected to be coeval. The difference in radiocarbon age may derive from the intrinsic problems in dating bulk soil samples. In fact these represent composite ages (e.g. an average age for all of the organics in the sample) and, frequently, may have experienced post-

depositional contamination with younger carbon that rejuvenates the true age [Matthews 1980; Polach *et al*. 1981; Rosholt *et al*. 1991].

On this light, if we consider reliable the older of the two measured ages, the ca. 100 m-stream deflections developed during the past 6720 ± 120 cal yr BP, after the final stage of deglaciation [Sowers and Bender, 1995; Hori et al., 2002], yields a slip rate of 15.7 ± 4 mm/yr.

4.2 The Beykoy-Degirmenbasi area

4.2.1. Measuring the offset

At the Beykoy-Degirmenbasi area, the Düzce Fault crosscuts a wide Pleistocene bajada that extend as far as 3 km north of the mountain-piedmont junction. Nowadays, this bajada is no more active and undergoes erosion, as testified by the entrenched streams that flow over it and by the overlap of young generation of alluvial fan onto the old deposited fan strata at the base of the range front. Here, the Düzce Fault presents a left step-over arrangement where the transpressional stress-field results in a 0.8 km-wide and 1.8 km-long pressure ridge (spot f, fig. 12 and fig. 13) and the oldest alluvial deposits reach the elevation of more than 130 m above the nearby Düzce Basin. This pressure ridge has asymmetric cross profile, with a steep northern flank and gentle southern flank. The northern flank was affected by the main 1999 coseismic ruptures that up-thrown of about 0.7 m the southern block [Akyuz et al., 2002; Duman et al., 2005; Pucci et al., 2006b], conversely the southern flank expresses a smoother transition to the suspended bajada surface.

West of this Pleistocene bajada the Develi River, that is one of the largest watercourse of the Düzce Basin drainage system, outflows from the

Almacik Block at around 210 m a.s.l. and, turning left, flows toward the Efteni Lake (fig. 5). The Develi River has a strong stream power and sediment load, as testified by intensely shaped erosional and depositional features (e.g. river terraces). North of the fault trace, we recognized four, clear-cut orders of climatically controlled terraces, whose present morphology mimics the Develi River left turn. The first order is the present-day terrace (I, fig. 12). The second order is an Holocene terrace, about 1.0 m higher than the present-day terrace (II, fig. 12). The third order is formed by a Late Pleistocene flight of alluvial fan deposits, 7-10 m higher than the Holocene terrace (III, fig. 12). The fourth order is the oldest and highest erosional terrace, 10-15 m higher than the third order (IV, fig. 12). The risers between the third and the fourth order terraces (III-IV, fig. 12) is incised in the Pleistocene bajada deposits and can be correlated with the one at the river outlet, where it is exposed the bedrock (spot e, fig. 12 and 13). The risers are found only at the right side of the river outlet and degrade toward the plain to the north according to the depositional gradient of the fan strata where they are down-cut in: from 280 m to 200 m a.s.l. and from 220 m to 200 m a.s.l., respectively.

On the basis of the present day morphology of alluvial fan remnant, we suppose the presence during the Pleistocene of a large fan, up to 2.5 km wide, at the Develi River outlet. These sediments have been later incised, reflecting climatic glacial-interglacial oscillations and related variations in sediment and water discharges. Presently, the Düzce Fault crosscutting the alluvial fan deposits, shifted them far away from the path of the river, and as a consequence sheltered terraces and risers to the north from erosion (figs. 14a, b, c and d). The Develi River has been sufficiently large to be able to

maintain its longitudinal profile by downcutting and keeping peace with the base-level changes, without preserving any fault-related stream deflection.

Since the third and the fourth order of risers were displaced, they have not been substantially modified, because the resultant juxtaposition did not engaged any other important stream (i.e. capture) or strong erosional process. Because of this, we were able to correlate risers at both sides of the fault and we reconstruct their tectonic evolution (fig. 12). For the fourth and the third order risers, we measured 890 ± 110 m and 300 ± 20 m offsets, respectively.

4.2.2. Dating

Since we expected probable ages close or out of the application limits of the radiocarbon dating method, we sampled the third and the fourth order of terrace risers for Optically Stimulated Luminescence (OSL) dating method. To avoid possible reoccupation and consequently rejuvenation of the surfaces, we sampled the highest terraces located south to the deformation (figs. 13 and 14). Numerous studies indicate the robustness of OSL method because it has yielded ages in agreement with other chronologic controls for at least the past c. 100 ka [Jain et al., 2003 and reference therein]. A luminescence age is a measure of the time elapsed since the last sunlight exposure of the sediment. The selection and sampling of sediment is the crucial step in the luminescence analysis. The alluvial fan presents clay-rich silt deposits amenable for dating. In fact, the alluvial sedimentary environment deposed relatively thick and homogeneous stratigraphic unit that has not undergone significant water-content variations or diagenetic changes during burial. We sampled sediment cores about 0.6 m below the surface, to insure stratigraphic and geologic luminescence

integrity, by hammering into the section, through a metal pipe, a black ABS pipe (5 cm diameter and 20 cm long), that we closed with end caps. In order to allow dose rate, mineralogic and granulometric analyses, we took additional 100 g samples from the same sampled layer that have not be shielded from light exposure. The samples were dated at the Luminescence Laboratory, Department of Earth and Environmental Sciences, University of Illinois at Chicago.

The intensity of the luminescence was calibrated in the laboratory (table 2) to yield an equivalent dose, which is divided by an estimate of the radioactivity that the sample received during burial (dose rate) to render a luminescence age. Equivalent dose was determined for all samples by the multiple aliquot additive dose method (MAAD) [e.g. Forman and Pierson, 2002], under infrared stimulation (880 ± 80 nm) on the fine-grained (4-11 micron) polymineral extract for all samples. Resulting ages are 60 170 ± 6280 yr BP and 21 700 ± 1850 yr BP for the upper and the lower terraces, respectively (IV and III, fig. 12) (1σ, table 2).

The ca. 300 and 890 m measured offset of the 20 kyr BP and 60 kyr BP-old terrace risers translate to slip rates of 15.2 ± 3.5 mm/yr and 14 ± 2.1 mm/yr, respectively.

4.3 The slip-rates

Although the calculated slip rates span ages from 7000 up to 60 000 yr BP, their values are similar. Interestingly, the mathematical linear regression that interpolates the slip rates yields 14.0 mm/yr with standard deviation ± 1.8 mm/yr. This suggests a constant slip rate for the last 60 000 yr (fig. 15).

Discussion and conclusions

The geomorphological mapping of the tectonic landforms related to the Düzce Fault activity provided new information on the slip rate of this part of the NAFZ. The geomorphic expression of the Düzce Fault presents long-term evidence of a slip localization of the bulk of the ongoing dextral displacement. In particular, the eastern section of the Düzce Fault shows a mature and straight E-W trend that suggests that it has been experiencing persistent 1999-like surface rupturing for repeated seismic cycles.

Along this mature fault section, we recognized four offset geomorphic markers for which we reconstructed the original morphology that has been dissected by the Düzce Fault motion. We mapped two streams that, once they begun to incise their alluvial deposits, were forced to deflect for a total of about 100 m. By means of radiocarbon method, we dated the alluvial deposits of the paleosurface that represent the onset of the deflection at last 6720 ± 120 yr BP. This age and the ca. 100 m of stream deflection developed at the end of last deglaciation yields a slip rate of 15.7 ± 4 mm/yr. In addition, we documented the Düzce Fault crosscutting the terrace risers incised by the Develi River over its Late Pleistocene alluvial deposition. Here, we correlated and measured the offset of the two oldest terrace risers of about 300 and 890 m. By means of Optically Stimulated Luminescence method, we dated the alluvial deposits of the terraces, which represent the onset of their right-lateral tectonic shift at 60 170 ± 6280 yr BP and 21 700

± 1850 yr BP. These ages and offsets translate to slip rates of 14 ± 2.1 mm/yr and 15.2 ± 3.5 mm/yr, respectively.

The evaluation, at different time scales, of the Düzce Fault slip-rates suggests a constant rate of deformation of 14.0 ± 1.8 mm/yr and disproves a time-variable model [Armijo et al., 1999; Hubert-Ferrari et al., 2002; Şengör et al., 2005] at least for the last 60 000 yr. Interestingly, although poorly constrained, slip rates inferred from paleoseismological investigations are of the same order of magnitude, ranging between 9 and 18 mm/yr for the past 2000 yr (see fig. 15).

Assuming that the strain accumulation due to the plate motion along this part of the NAFZ, GPS measured (at short time-scales), is 1) relatively uniform and constant over the last 60,000 yr, and 2) completely released only by the Mudurnu (to the south) and the Düzce (to the north), parallel faults strands (fig. 3), imply that the Düzce Fault accommodates more than half of the total GPS slip-rate estimates. This indicates that the Düzce Fault importantly participates to the North Anatolian margin deformation. Moreover, this present-day partitioning of displacements rates between the Mudurnu and the Düzce faults configures a duplex [Woodcock and Fischer, 1986] as structural style of this part of the NAFZ active deformation. If this is the case, not only the Düzce Fault assumes a relevant role in the seismic hazard of the area that should be comparable to that of the Mudurnu Fault, but also arises the need to investigate the temporal fault interactions between the Mudurnu and the Düzce faults, as an interlinked seismogenic system. In addition, this observation should trigger further studies to understand the reason that drives such structural style along this part of the NAFZ and how it took place in the plate boundary evolution.

The increase of the geological offset observations is crucial to answer to one of the most important questions regarding the significance of the measurements of active surface deformation in the continental lithosphere: what is the relationship between strain accumulation and strain release? On short time scales (years), both strain accumulation and release are monitored using high-precision space-geodetic techniques (GPS; InSAR, etc.). However, on longer time scales (e.g., thousands of years, duration of interseismic intervals), strain accumulation measurements are derived only from geologic strain release data as proxies. In contrast to geodetic surface strain data, these geological data may be used as a direct measure of temporal and spatial variations of fault slip in the past. Such data spanning over long temporal or spatial scales are necessary to rule out either possibility due to the lack of reliable information about the amount and distribution of finite strain along the NAFZ and, consequently to reveal the NAFZ history.

Acknowledgements

This research is supported by the European Commission Project "Relief": Large earthquake faulting and implications for seismic hazard assessment in Europe: The Izmit-Düzce earthquake sequence of 1999, Turkey, Mw 7.4, 7.1, EVG1-CT-2002-00069.

References

Akyüz, H.S., A.A. Barka, E. Altunel, R.D. Hartleb, and G. Sunal, 2000. Field observations and slip distribution of the November 12, 1999 Düzce earthquake (M=7.1), Bolu - Turkey. In: A.A. Barka et al. (Eds.), The 1999 Izmit and Düzce earthquakes; preliminary results. Istanbul Technical University, Istanbul, Turkey, pp. 63-70.

Akyüz, H.S., R.D. Hartleb, A.A. Barka, E. Altunel, G. Sunal, B. Meyer and R. Armijo, 2002. Surface rupture and slip distribution of the 12 November 1999 Düzce earthquake (M7.1), North Anatolian Fault, Bolu, Turkey. Bulletin of the Seismological Society of America 92 (1), 61-66.

Aitken, M.J. and S.G.E. Bowman, 1975. Thermoluminescent dating: Assessment of alpha particle contribution. Archaeometry 17, 132-138.

Allen, C.R., 1962. Circum-Pacific faulting in the Philippines–Taiwan region. J. Geophy. Res. 67, 4795–4812.

Ambraseys, N.N., 1970. Some characteristic features of the North Anatolian fault zone. Tectonophysics 9, 143-165.

Ambraseys N.N, 2002. The seismic activity of the Marmara Sea region over the last 2000 years. Bulletin of the Seismological Society of America 92 (1), 1-18.

Ambraseys N.N. and C.F. Finkel, 1995. The seismicity of Turkey and adjacent areas: a historical review, 1500-1800, Muhittin Salih Eren, 240 pp., Istanbul.

Armijo R., B. Meyer, A. Hubert and A.A. Barka, 1999. Westward propagation of the North Anatolian fault into the northern Aegean: Timing and kinematics. Geology 27 (3), 267-270.

Ayhan, M.A., C. Demir, A. Kilicoglu, I. Sanli, and S.M. Nakiboglu, 1999. Crustal motion around the western segment of the north Anatolian fault zone: geodetic measurements and geophysical interpretation. International Union of Geodesy and Geo-physics (IUGG99), Birmingham, United Kingdom, 18-30 July.

Ayhan, M.E., R.B¨urgmann, S. McClusky, O. Lenk, B. Aktug, E. Herece and R.E. Reilinger, 2001. Kinematics of the Mw = 7.2, 12 November 1999, Düzce, Turkey earthquake. Geophys. Res. Lett. 28 (2), 367-370.

Barka, A.A., 1992. The North Anatolian fault zone. Annales Tectonicae 6, 164-195.

Barka A.A. and K. Kadinski-Cade, 1988. Strike-slip fault geometry in Turkey and its influence on earthquake activity. Tectonophysics 7, 663-684.

Barka, A.A. and L. Gulen, 1989. Complex evolution of the Erzincan Basin (eastern Turkey). J. Struct. Geol. 11 (3), 275-283.

Canitez, N. and B. Ucer, 1967. Computer determinations for the fault plane solutions in and near Anatolia. Tectonophysics 4, 235-244.

Dewey, J.F., M.R. Hempton, W.S.F. Kidd, F. Saroglu and A.M.C. Şengör, 1986. Shortening of continental lithosphere; the neotectonics of eastern Anatolia, a young collision zone. Geological Society Spec. Pub. 19, 3-36.

Dhont, D., J. Chorowicz, T. Yürür, O. Köse, 1998. Polyphased block tectonics along the North Anatolian Fault in the Tosya basin area (Turkey). Tectonophysics 299, 213–227.

Duman, T., Ö. Emre, A. Dogan and S., 2005. Step-over and bend structures along the 1999 Düzce earthquake surface rupture, North Anatolian Fault, Turkey. Bull. Seism. Soc. Am. 95 (4), 1250-1262.

Emre, Ö., T. Erkal, A. Tchepalyga, N. Kazancı, M. Keçer and E. Ünay, 1998. Doğu Marmara bölgesinin Neojen-Kuaternerdeki evrimi. Maden Tetk. Arama Derg. 120, 289–314. (in Turkish)

Erin¸c, S., 1953. Doğu Anadolu Coğrafyası: Istanbul Univ. Yayın No. 572, Istanbul Univ. Edeb. Fak. Coğraf. Enst. Yayin, 15, Istanbul, pp. 124. (in Turkish)

Forman, S.L., and J. Pierson, 2002. Late Pleistocene luminescence chronology of loess deposition in the Missouri and Mississippi river valleys,

United States. Palaeogeography Palaeoclimatology Palaeoecology 186 (1-2), 25-46.

Fu, B., Y. Awata, J. Du, W. He, 2005. Late Quaternary systematic stream offsets caused by repeated large seismic events along the Kunlun fault, northern Tibet. Geomorphology 71, 278– 292.

Gaudemer, Y., P. Tapponnier and D.L. Turcotte, 1989. River offsets across active strike-slip faults. Annales Tectonicae 3 (2), 55-76.

Herece, E., and E. Akay, 2003. 1:100.000 geological maps of the North Anatolian Fault, *General Directorate of Mineral Research and Exploration*, Ankara, Appendix 3 and 4.

Hori, K., Saito, Y., Zhao, Q., Wang, P., 2002. Control of incised-valley fill stacking patterns by accelerated and decelerated sea-level rise: Changjiang example during the last deglaciation. Geo-Marine Letters 22 (3), 127-132.

Huang, W., 1993. Morphologic patterns of stream channels on the active Yishi Fault, southern Shandong Province, eastern China: implication for repeated great earthquakes in the Holocene. Tectonophysics 219, 283– 304.

Hubert-Ferrari, A., R. Armijo, G. King, B. Meyer and A. Barka, 2002. Morphology, displacement, and slip rates along the northern Anatolian Fault, Turkey. J. Geophys. Res. 107 (B10), 2235, doi: 10.1029/2001JB000393.

Hubert-Ferrari, A., G. King, I. Manighetti, R. Armijo, B. Meyer and P. Tapponnier, 2003. Long-term elasticity in the continental lithosphere; modelling the Aden Ridge propagation and the Anatolian extrusion process. Geoph. J. Int. 153 (1), 111-132.

Jackson, J. and D. McKenzie, 1988. The relationship between plate motions and seismic moment tensors, and the rates of active deformation in the Mediterranean and Middle East. Geoph. J. Int. 93 (1), 45-73.

Jackson, J., R. Norris, J. Youngson, 1996. The structural evolution of active fault and fold systems in central Otago, New Zealand: evidence revealed by drainage patterns. Journal of Structural Geology 18, 217– 234.

Jain, M., L. Botter-Jensen and A.K. Singhvi, 2003. Dose evaluation using multiple-aliquot quartz OSL: test of methods and a new protocol for improved accuracy and precision. Radiation Measurements 37, 67-80.

Johnson, A. M., R. W. Fleming, and K. M. Cruikshank, 1994. Shear zones formed along long, straight traces of fault zones during the 28 June 1992 Landers, California, earthquake. Bull. Seism. Soc. Am. 84**,** 499–510.

Kahle H. G., M. Cocard, Y. Peter, A. Geiger, R. Reilinger, S.C. McClusky, R. King, A. Barka and G. Veis, 1999. GPS-derived strain rate field within the boundary zones of the Eurasian, African, and Arabian Plates. J. Geophy. Res. 105 (B3), 23 353-23 370.

Kahle H. G., M. Cocard, Y. Peter, A. Geiger, R. Reilinger, A. Barka and G. Veis, 2000. GPS-derived strain rate field within the boundary zones of the Eurasian, African, and Arabian Plates. J. Geophy. Res. 105 (B3), 23 353-23 370.

Keller, E.A., M.S. Bonkowski, R.J. Korsch and R.J. Shlemon, 1982. Tectonic geomorphology of the San Andreas fault zone in the southern Indio Hills, Coachella Valley, California. Geol. Soc. Am. Bull. 93, 46-56.

Komut T., 2005. Paleoseismological studies on Düzce fault and geological data on the seismogenic sources in the vicinity of Düzce area, Kandilli Observatory and Earthquake Research Institute Boğaziçi University, Ph.D. Thesis, pp. 155.

Ikeda, Y, Y. Suzuki, E. Herece, F. Saroglu, A.M. Isikara and Y. Honkura, 1991. Geological evidence for the last two faulting events on the North Anatolian fault zone in the Mudurnu Valley, western Turkey. Tectonophysics 193 (4), 335-345.

IrrlitzW., 1972. Lithostratigraphie und tektonische Entwicklung des Neogens in Nordostanatolien (Känozoikum und Braunkohlen in der Türkei. 6.). Beih. Geol. Jahrb. 120, 111 pp.+10 plates. (in German)

Lazarte, C.A., J.D. Bray, A.M. Johnson, and R.E. Lemmer, 1994. Surface breakage of the 1992 Landers earthquake and its effects on structures. Bull. Seism. Soc. Am 84**,** 547–561.

Le Pichon, X., A.M.C. Şengör, E. Demirbag, C. Rangin, C. İmren, R. Armijo, N. Görür, N. Çağatay, B. Mercier de Lepinay, B. Meyer, R. Saatçılar and B. Tok, 2001. The active Main Marmara Fault. Earth and Planetary Science Letters 192, 595-616.

Matsuda T., 1967. Cumulative displacement of river gorges by active fault Journal of the Geological Society of Japan 73 (2), pp.121.

Matthews, J. A, 1980. Some problems and implication of 14C dates from a podzol buried beneath an end moraine at Haugabreen, southern Norway. Geografiska Annaler 62°, 185-208.

McClusky, S.C., A. Balassanian, A.A. Barka, C. Demir and S. Ergintav, 2000. Global positioning system constrain on plate kinematics and dynamics in the eastern Medditerranean and Caucasus. J. Geophy. Res. 105 (B3), 5695-5720.

McKenzie, D.P., 1972. Active tectonics of the Mediterranean region. Geophys. J. R. Astron. Soc. 30, 109-185.

Okay, A.İ., 1989. Tectonic units and sutures in the Pontides, northern Turkey: in: A.M.C. Şengör (Ed.), Tectonic evolution of the Tethyan Region. London, Kluwer Academic Publishers 109-116

Okay, A.l., E. Demirbag, H. Kurt, N. Okay, I. Kuscu, 1999. An active, deep marine strike-slip basin along the North Anatolian Fault in Turkey. Tectonics 18 (1), 129-147

Ouchi, S., 2004. Flume experiments on the horizontal stream offset by a strike-slip fault. Earth Surface Processes and Landforms 29, 161– 173.

Ouchi, S., 2005. Development of offset channels across the San Andreas fault. Geomorphology 70, 112– 128.

Palyvos N., D. Pantosti, C. Zabci, G. D'Addezio, 2006. Late Holocene earthquakes at the Mudurnu valley, 1967 earthquake segment of the North Anatolian Fault Zone, recorded in river channel deposits. Bull. Seism. Soc. Am.. (submitted).

Pantosti, D., S. Pucci, N. Palyvos, P.M. De Martini, G. D'Addezio and C. Zabci, 2006. Paleoseismological investigations along the Düzce Fault (Turkey, Ms 7.1, Nov. 1999). Bull. Seism. Soc. Am.. (submitted).

Polach, H., J. Golson, and J. Head, 1981. Radiocarbon Dating: A Guide for Archaeologists on the Collection and Submission of Samples and Age-Reporting Practices, in Australian Field Archaeology: A Guide to

Techniques. Australian Institute of Aboriginal Studies. Canberra, Australia, 145-152.

Polonia A., L. Gasperini, A. Amorosi, E. Bonatti, G. Bortoluzzi, N. Çagatay, L. Capotondi, M.-H. Cormier, N. Görür, C. McHugh, L. Seeber, 2004. Holocene slip rate of the North Anatolian Fault beneath the Sea of Marmara. Earth and Planetary Science Letters 227, 411– 426.

Pucci, S., Palyvos, N., Zabci, C., Pantosti, D., and M. Barchi, 2006a. Coseismic ruptures and tectonic landforms along the Düzce segment of the North Anatolian Fault Zone (Ms 7.1, Nov. 1999). J. Geophys. Res. (in press).

Pucci S., D. Pantosti, M. Barchi and N. Palyvos, 2006b. Evolution and complexity of the seismogenic Düzce fault zone (Turkey) depicted by coseismic ruptures, Plio-Quaternary structural pattern and geomorphology. Earth Planet. Sci. Lett., submitted.

Reid, H.F., 1910. The California earthquake of April 18, 1906, The mechanics of the earthquake. Report of the (California) State Earthquake Investigation Commission, Sacramento 2, Publ. 87, 1-192.

Reimer, P.J., M.G.L. Baillie, E. Bard, A. Bayliss, J.W. Beck, C. Bertrand, P.G. Blackwell, C.E. Buck, G. Burr, K.B. Cutler, P.E. Damon, R.L. Edwards, R.G. Fairbanks, M. Friedrich, T.P. Guilderson, K.A. Hughen, B. Kromer, F.G. McCormac, S. Manning, C. Bronk Ramsey, R.W. Reimer, S.

Remmele, J.R. Southon, M. Stuiver, S. Talamo, F.W. Taylor, J van der Plicht and C.E. Weyhenmeyer, 2004. IntCal04 terrestrial radiocarbon age calibration, 0-26 cal kyr BP. Radiocarbon 46, 1029-1058.

Reilinger, R.E., S.C. McClusky, M.B. Oral, W. King and M.N. Toksöz, 1997. Global Positioning, System measurements of present-day crustal movements in the Arabian-Africa-Eurasia plate collision zone. J. Geophy. Res. 102 (B5), 9983-9999.

Reilinger, R.E., Toksöz, M.N., McClusky and A.A. Barka, 2000. 1999 Izmit, Turkey Earthquake was no surprise. GSA Today 10, 1-6.

Reinecker, J., O. Heidbach, M. Tingay, P. Connolly, and B. Müller, 2004. The 2004 release of the World Stress Map (available online at www.world-stress-map.org)

Rosholt, J.N., S.M. Colman, M. Stuiver, P.E. Damon, C.W. Naeser, N.D. Naeser, B.J. Szabo, D.J. Muhs, J.C. Liddicoat, S.L. Forman, M.N. Machette, and K.L. Pierce, 1991. Dating methods applicable to the Quaternary. In: Morrison, R.B., (Ed.), Dating Methods Applicable to the Quaternary. The Geology of North America, vol. K-2, 45-74. Geological Society of America, Boulder, Colorado.

Şaroğlu, F., Ö. Emre and İ. Kuşçu, 1992. Active fault map of Turkey. General Directorate of Mineral Research and Exploration, Ankara.

Schwartz, D.P., and K.J. Coppersmith, 1984. Fault behavior and characteristic earthquake: examples from the Wasatch and San Andreas fault zones. J. Geophys. Res. 89, 5681-5698.

Şengör, A.M.C., 1979. The North Anatolian transform fault: Its age, offset and tectonic significance. J. Geol. Soc. London 136, 269-282.

Şengör, A.M.C., N. Görür and F. Şaroğlu, 1985. Strike-slip faulting and related basin formation in zones of tectonic escape; Turkey as a case study. In Biddle, K.T., and N. Christie-Blick (Eds.) Strike-slip Deformation, Basin Formation and Sedimentation, Soc. Econ. Paleont. Min. Spec. Publ. 37, 227-264.

Şengör, A.M.C., O. Tüysüz, C. İmren, M. Sakınç, H. Eyidoğan, N. Görür, X. Le Pichon and C. Rangin, 2005. The North Anatolian Fault: a new look. Annu. Rev. Earth Planet. Sci. 33, 37-112.

Şengör, A.M.C. and Yılmaz, Y., 1981. Tethyan evolution of Turkey; a plate tectonic Approach. Tectonophysics 75, 181-241.

Seymen, I., 1975. Tectonic characteristics of the North Anatolian fault zone in the Kelkit valley, Ph.D. thesis, Istanbul Technical Univ., Istanbul, Turkey, 192 pp.

Shimazaki, K., and T. Nakata, 1980. Time-predictable recurrence model for large earthquakes. Geophys. Res. Lett. 7, 279-282.

Sieh, K.E., R.H. Jahns, 1984. Holocene activity of the San Andreas fault at Wallace Creek, California. Geol. Soc. Am. Bull. 95, 883– 896.

Sieh, K.L., L. Jones, E. Hauksson, K. Hudnut, D. Eberhart-Phillips, T.H. Heaton, S. Hough, K. Hutton, H. Kanamori, A. Lilje, S. Lindvall, S.F. McGill, J. Mori, C. Rubin, J.A. Spotila, J. Stock, H.K. Thio, J. Treiman, B. Wernicke, and J. Zachariasen, 1993. Near-field investigations of the Landers earthquake sequence, April to July, 1992. Science 260**,** 171–176.

Sowers, T.A. and M. Bender, 1995, Climate records during the last deglaciation. Science 269, 210-214.

Strahler, A.N., 1952. Dynamic basis of geomorphology. Geol. Soc. Am. Bull. 63, 923-938.

Straub, C., H. G. Kahle, and C. Schindler, 1997. GPS and geologic estimates of the tectonic activity in the Marmara Sea region, NW Anatolia. J. Geophys. Res. 102 (B12), 27 587-27 601.

Stuiver, M., and P.J. Reimer, 1993. Extended (super 14) C data base and revised CALIB 3.0 (super 14) C age calibration program. Radiocarbon 35, 215-230.

Tatar Y., 1978. Kuzey Anadolu Fay Zonunun Erzincan-Refahiye arasindaki bölümü üzerinde tektonik incelemeler. Yerbilimleri 4, 201–36.(in Turkish)

Tchalenko, J.S., and N.N. Ambraseys, 1970. Structural analysis of the Dasht-e Bayaz, Iran, earthquake fractures. Geol. Soc. Am. Bull. 81, 41–60.

Tchalenko, J.S., and M. Berberian, 1975. Dasht-e Bayaz fault, Iran: earthquake and earler related structures in bedrock. Geol. Soc. Am. Bull. 86, 703–709.

Wallace, R.E., 1968. Notes on stream channels offset by the San Andreas fault, southern Coast Ranges, California. In: Dickinson, W.R., and A. Grantz (Eds.), Conference on Geologic Problems of the San Andreas Fault System. Stanford University Publication in Geological Sciences 11, 6– 21.

Wallace, R.E., 1987. Grouping and migration of surface faulting and variation in slip rates on faults in the Great Basin province, Bull. Seism. Soc. Am. 77, 868-877.

Westaway, R., 1994. Present-day kinematics of the Middle-East and Eastern Mediterranean. J. Geophys. Res. 99, 12 071-12 090.

Wong, H K, T. Luedmann, A. Ulug and N. Gorur, 1995. The Sea of Marmara; a plate boundary sea in an escape tectonic regime. Tectonophysics 244 (4), 231-250.

Woodcock, N.H., and M. Fischer, 1986. Strike-slip duplexes. J. Struct. Geol. 8 (7), 725-735.

Yilmaz, A. and H.S. Yilmaz, 2004. Geology and Structural Evolution of the Tokat Massif (Eastern Pontides, Turkey). Turkish J. Earth Sci. 13, 231-246.

Yoshioka, T., K. Okumura and I. Kuscu, 1991. Trench excavation of the North Anatolian Fault, Turkey. Chishitsu News 4 (440), 60-66.

Captions

Figure 1

Tectonic setting of the eastern Mediterranean and continental extrusion of the Anatolian plate. Current motion relative to Eurasia (GPS [Global Positioning System] and SLR [Satellite Laser Ranging] velocity vectors, in mm/yr, from Reilinger et al., 1997)(modified from Armijo et al., 1999).

Figure 2

a) Slip rates distribution along the North Anatolian Fault Zone (NAFZ). Different symbols are used on the basis of the time-scale and type of measured offset. Thin bars indicate uncertainties of the measurements. b) Location of the slip rate measures along the NAFZ. Numbers refer to slip rates from: (1) Armijo et al. [1999]; (2) Polonia et al. [2004]; (3) and (5) [Hubert-Ferrari et al., 2002]; (4) Dhont et al. [1998]; (6) to (9), (12) and (13) Erinc [1953], Gaudemer et al. [1989], Barka and Gulen, [1989], Huber-Ferrari et al. [2002] and Şengör et al. [2005]; (10) and (11) Irrlitz [1972], Seymen [1975], Tatar [1978], Barka, [1992], Westaway [1994] and Hubert-Ferrari et al. [2002].

Figure 3

The Izmit and Düzce earthquake ruptures (modified from Akyuz et al. [2002]). Epicenter location (stars) and focal mechanism solutions from Harvard CMT. Inset locates the region of the NAFZ affected by the 1999 seismic sequence.

Figure 4

The Düzce coseismic fault trace can be divided in two parts depending on its geometry (see Pucci et al. [2006b]). The eastern part shows localized slip. Late Pliocene-Holocene continental deposits (compilation by 1:20 000 scale field survey and by Herece and Akay [2003]) and main drainage features of the Düzce basin are reported. Shaded relief based on digital elevation model (DEM, interpolated from 10 m contours and auxiliary 5 m contours of 1:25 000 scale topographic maps). Contour interval 100 m. (see fig. 3 for location).

Figure 5

Simplified geomorphological and coseismic fault scarp map of the two parts of the Düzce Fault. a) Western section. b) Eastern section. Continental deposits from 1:20 000 scale field survey, bedrock from Herece and Akay [2003]. Letters indicate locations discussed in the text. Contour interval 100 m. (see fig. 4 for location).

Figure 6

a) View of a cross-section of a tectonic ridge along the Düzce Fault. Black arrows point to the 1999 ruptures. b) Close up of the deformed Quaternary fan deposits outcropping at the tectonic ridge. The deformation zone mainly shows transpressional structures with apparent transtensional structures caused by the juxtaposition of the strike-slip motion. Dotted circle indicate the block moving out of the picture. (see fig. 5 for location).

Figure 7

Simplified geomorphological map of the Tilki-Cicubey area. Contour interval 10 m. Letters indicate locations discussed in the text. (see fig. 5 for location).

Figure 8

a) Schematic illustration showing evolution of an apparent offset of a stream opposite to the sense of strike-slip motion due to stream capture. b) Measurement of a stream channel offset across a right-lateral strike-slip fault. (modified from Fu et al. [2005]).

Figure 9

Views of the Amcahasanbey site (1 in fig. 7). a) aerial view of the deflected stream and its channel wall. b) view of the tectonic ridge and of the dammed area. Small black arrows point to the coseismic rupture trace. Hexagon indicates the radiocarbon sample location. (see fig. 7 for view directions).

Figure 10

Schematic reconstruction of the recent stream history at the Amcahasanbey site (1 in fig. 7). a) Late Pleistocene-Early Holocene. The stream flows and deposits along a quasi-straight channel; b) Holocene (ca. 7000 yr). The stream starts to incise; c) Present. The stream is entrenched and right-hand deflected by the fault. The piercing points (x, y and w) used to measure the stream deflection are reported. (see fig. 7 for location).

Figure 11

Aerial view of the deflected stream at the Cicubey site (2 in fig. 7). Small black arrows point to the coseismic rupture trace. Hexagon indicates the radiocarbon sample location. (see fig. 7 for view direction).

Figure 12

Simplified geomorphological map of the Beykoy-Degirmenbasi area. Contour interval 10 m. (see fig. 5 for location).

Figure 13

View of the pressure ridge and the terrace risers at the Beykoy-Degirmenbasi area. Little black arrows point to the coseismic rupture trace. Hexagonal symbol indicates the sample locations. (see fig. 12 for view direction).

Figure 14

Schematic chronological reconstruction of the geometry of the Beykoy-Degirmenbasi area. Düzce Fault has been crosscutting and right-laterally shifting the terrace flights and risers of the north-eastern side, that were sheltered from erosion. a) Late Pleistocene. The Develi River deposit a large alluvial fan, building a bajada at the base of the range front; b) Late Pleistocene (60 to 20 kyr). The Develi River starts to incise the fourth order terrace deposits (IV) and to construct the younger, lower third order terrace (III) until 20 kyr; c) Late Pleistocene (20 kyr) to Holocene. The Develi River starts to incise the Late Pleistocene (20 kyr) third order terrace (III) and to construct the Holocene terrace (II). d) Late Holocene. The Develi

River incises the Holocene deposits of the second order (II) and to construct the present terrace (I). Risers IV-III and III-II are all severely offset.

Figure 15

Slip rate diagram of the Düzce Fault. The slip rates calculated at different time-scales are reported along with the interpolated uniform slip rate.

Table 1.

Radiocarbon ages and associated chronologic data for sediments from the Tilki-Cicubey area. The calibrated ages are calculated for the probability density function at the 95.4 per cent confidence limit (2σ).

Table 2.

Optically stimulated luminescence (OSL) ages and associated chronologic data for sediments from the Beykoy-Degirmenbasi area. [a)] Blue emissions are measured with 3-mm-thick Schott BG-39 and one, 3-mm-thick Corning 7-59 glass filters that blocks >90% luminescence emitted below 390 nm and above 490 nm in front of the photomultiplier tube. [b)] The stability of the laboratory beta-induced (Gy) luminescence signal after preheating and storage was tested by comparing luminescence emissions of immediately after preheating (10 hours at 150 °C) and with at least a 30 day storage. A thermal stability ratio 1.06 -0.94 indicates little or no signal instability, within analytical resolution. [c)] Measured alpha efficiency factor as defined by Aitken and Bowman [1975]. [d)] U and Th values calculated from alpha count rate, assuming secular equilibrium. K20 % determined by ICP-MS,

Activation Laboratory Ltd., Ontario. [e)] Contains a cosmic rate dose rate component of 0.20 ± 0.02. [f)] All errors are at one sigma.

Figure1
Click here to download high resolution image

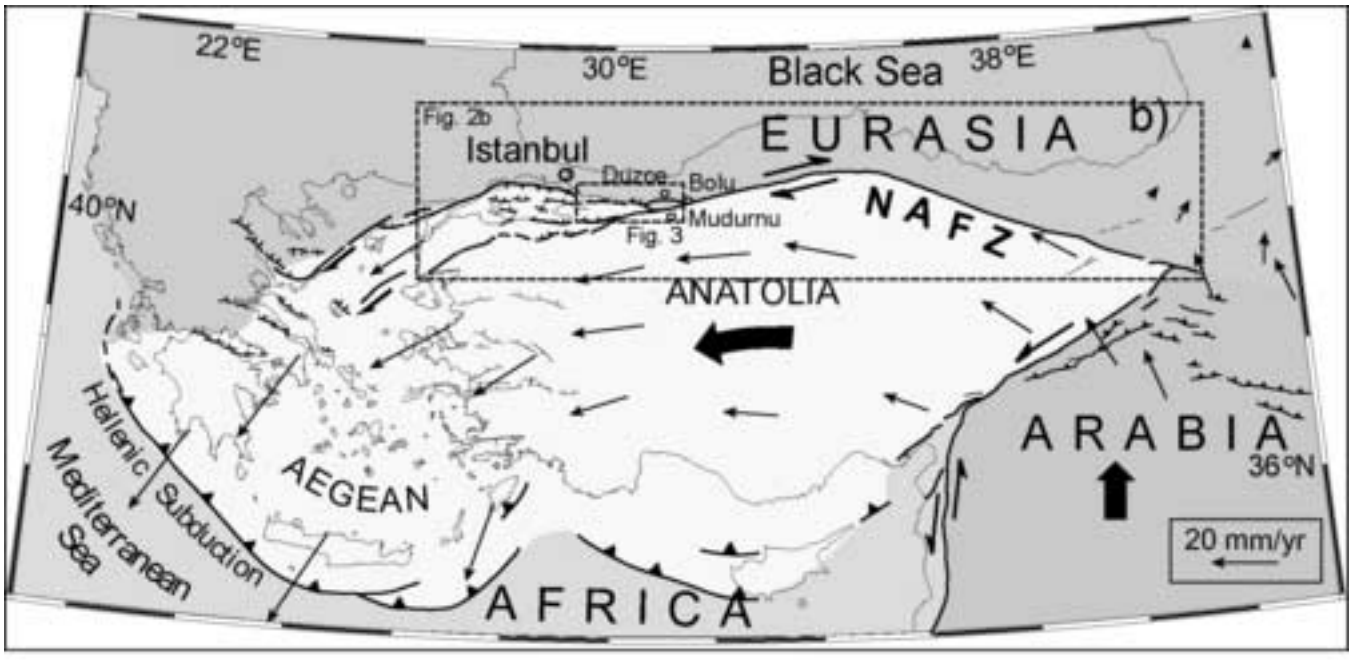

Fig. 1

Figure2
Click here to download high resolution image

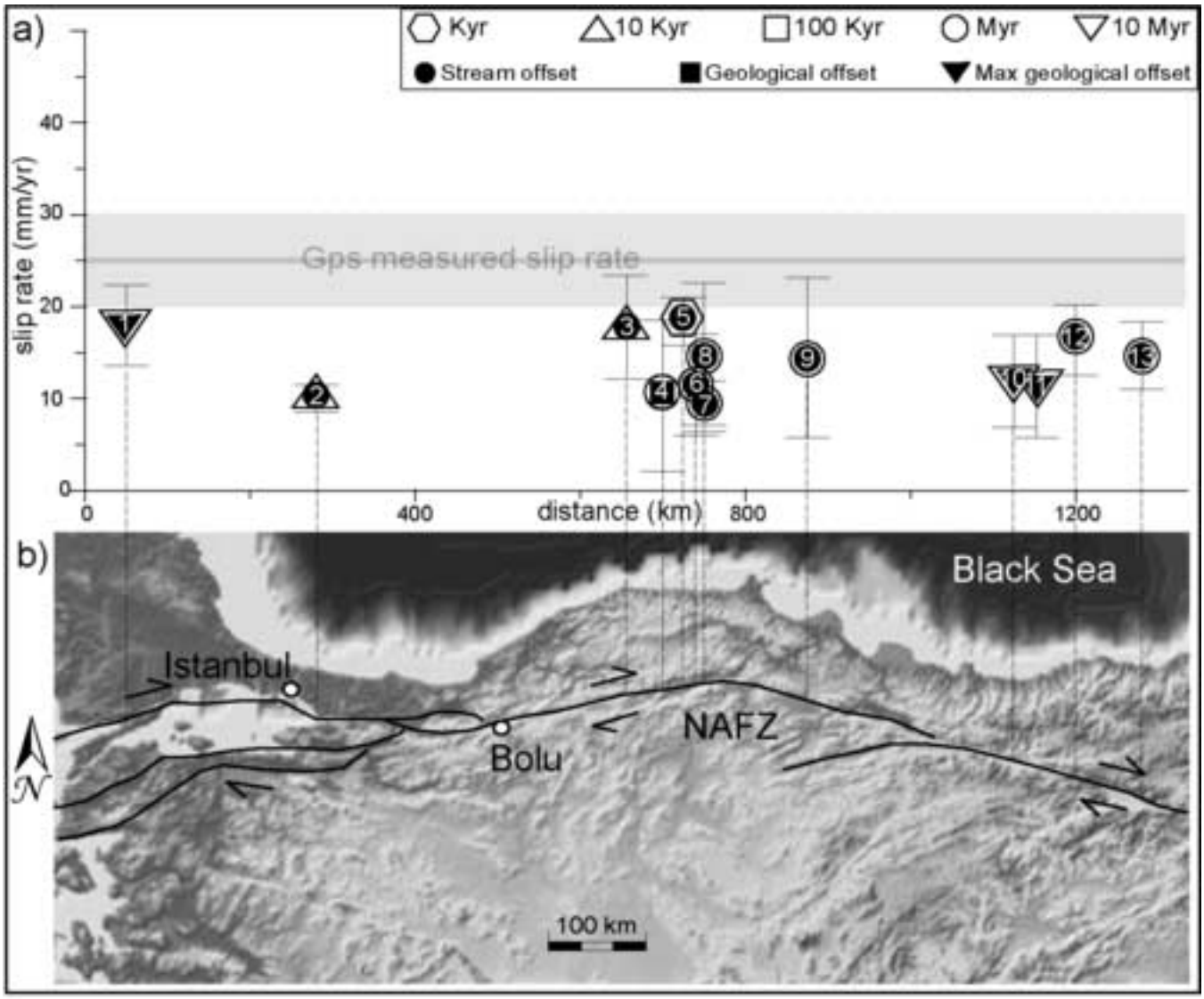

Fig. 2

Figure3
Click here to download high resolution image

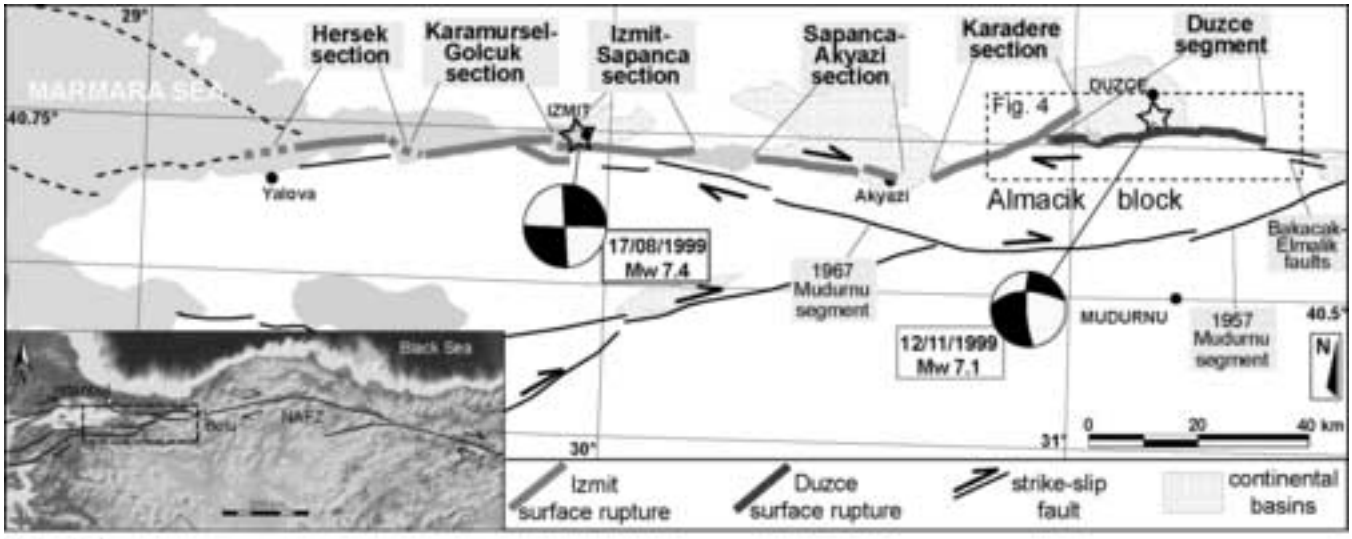

Fig. 3

Figure 4

Click here to download high resolution image

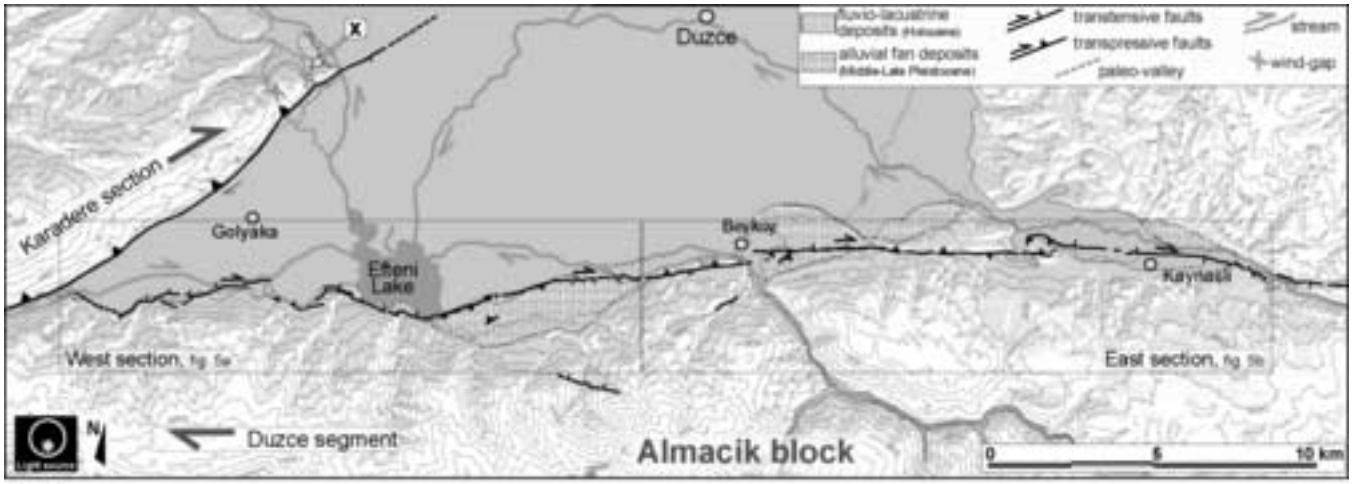

Fig. 4

Figure 5

Click here to download high resolution image

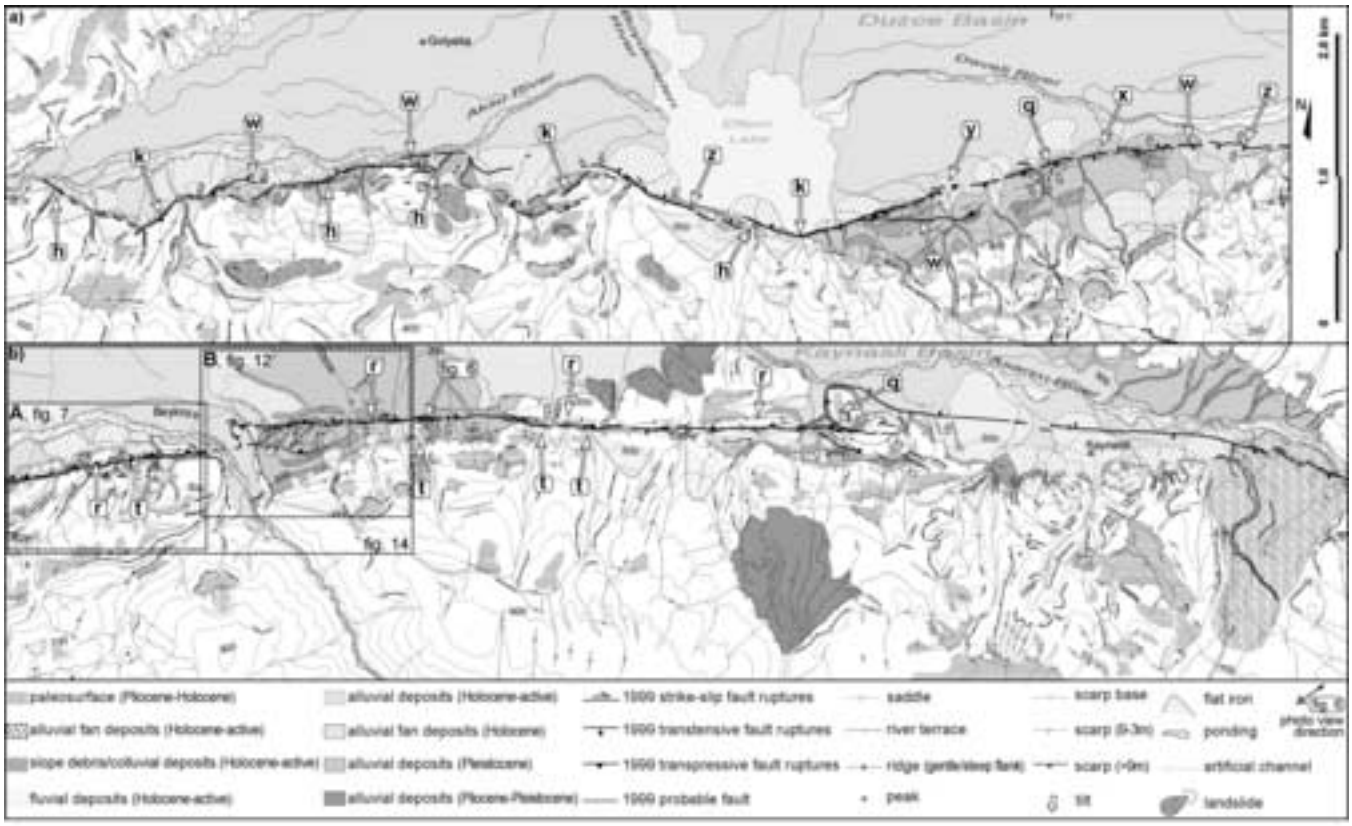

Fig. 5

Figure 6
Click here to download high resolution image

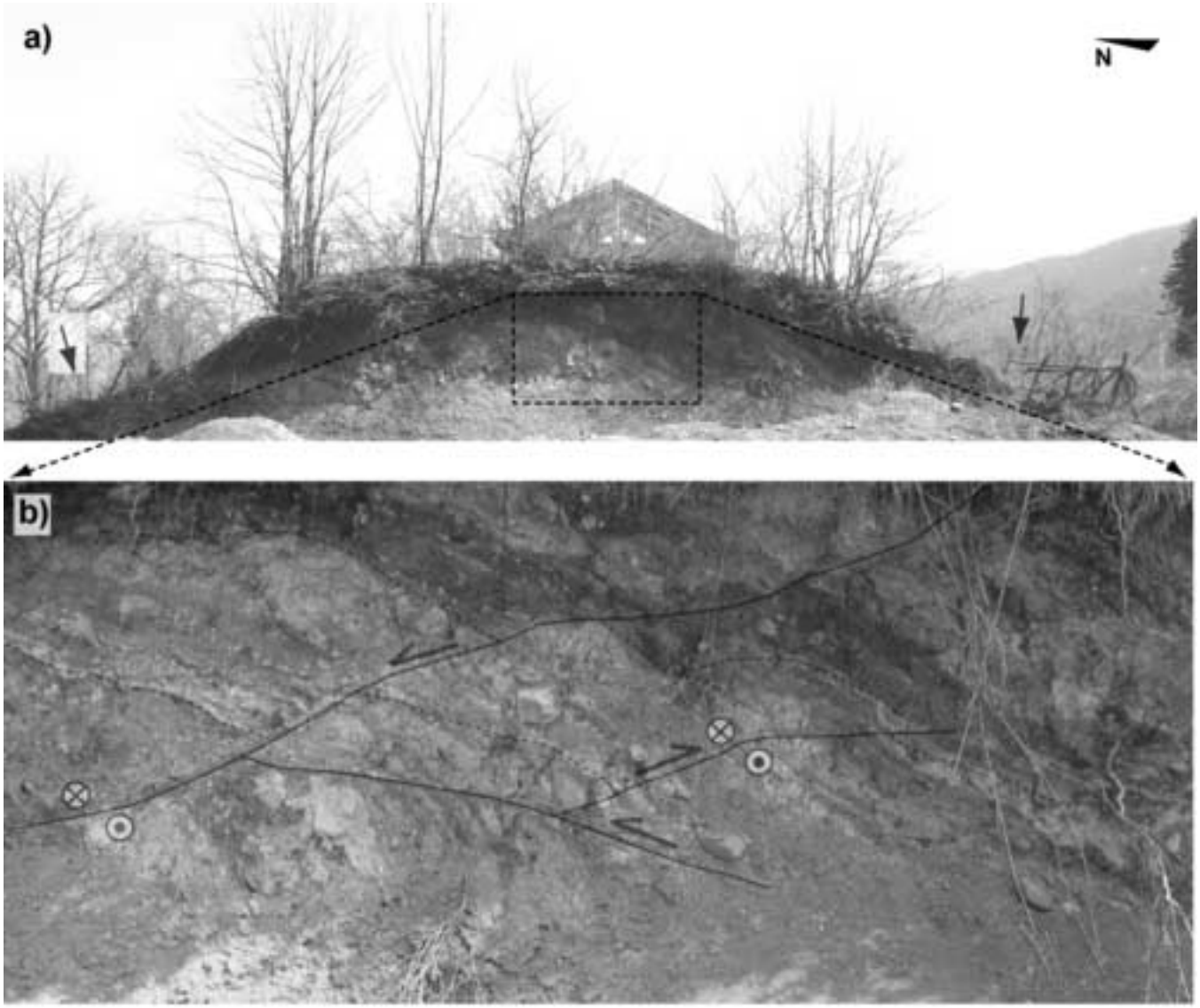

Fig. 6

Figure 7
Click here to download high resolution image

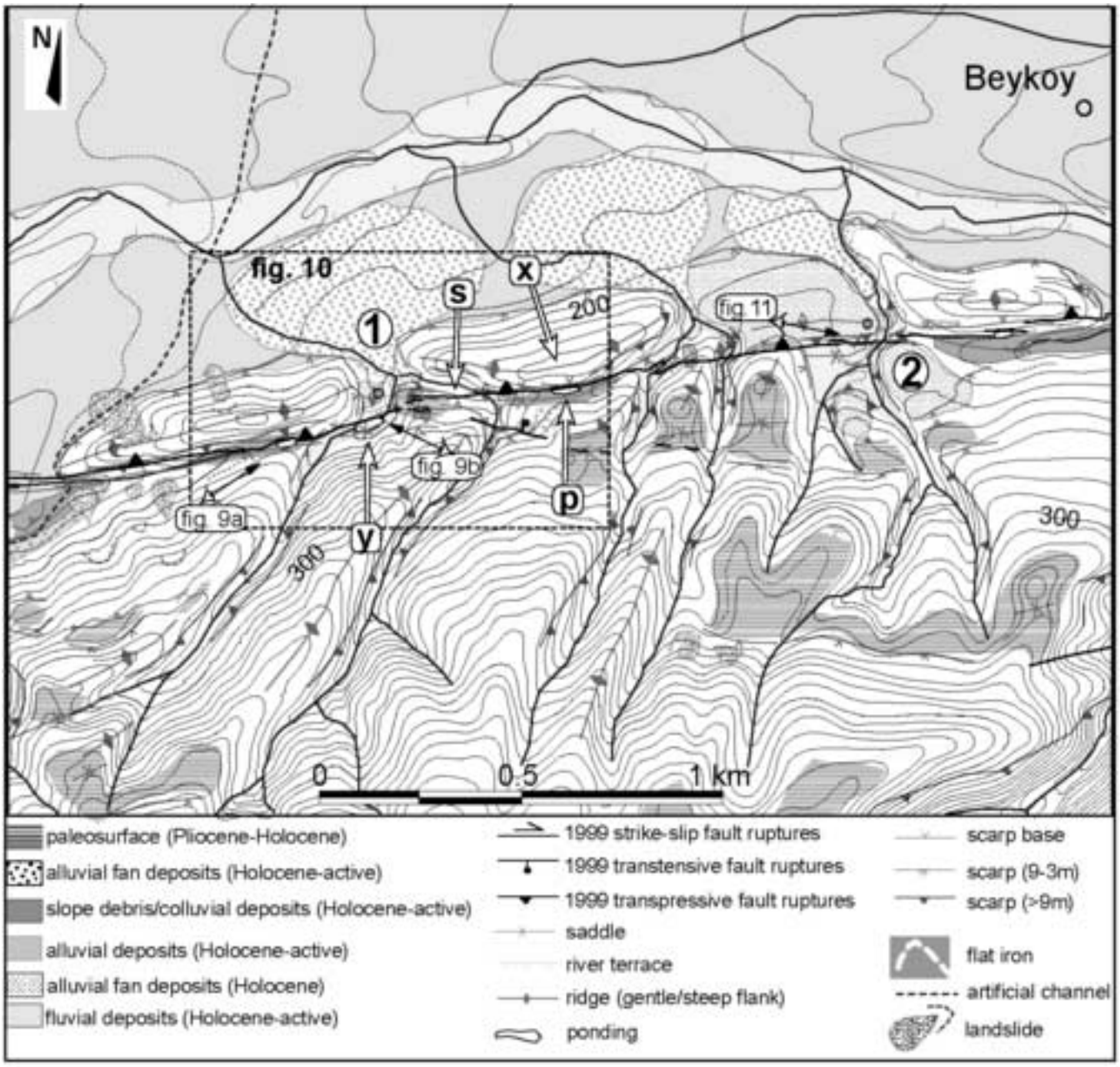

Fig. 7

Figure 8

Click here to download high resolution image

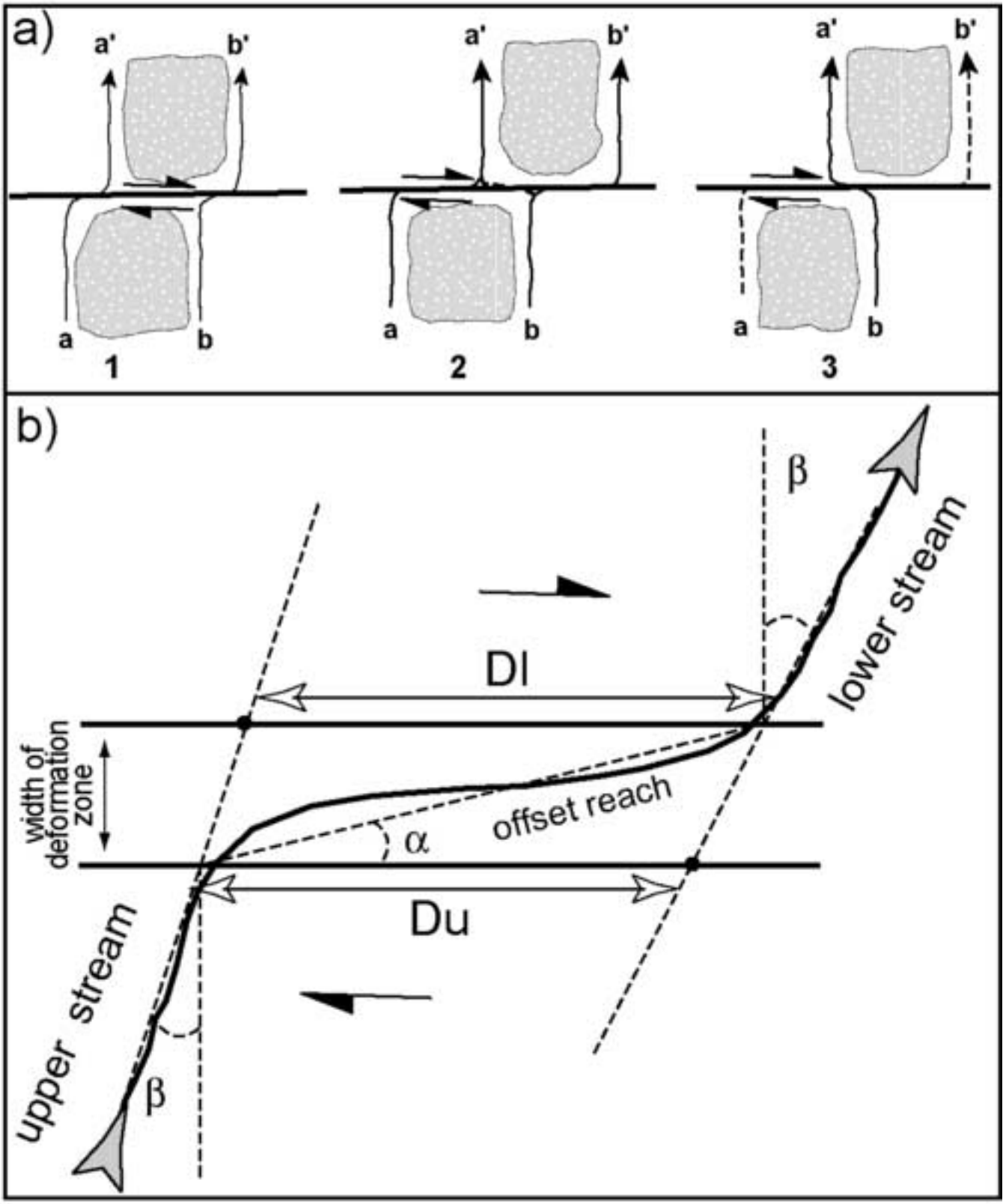

Fig. 8

Figure 9
Click here to download high resolution image

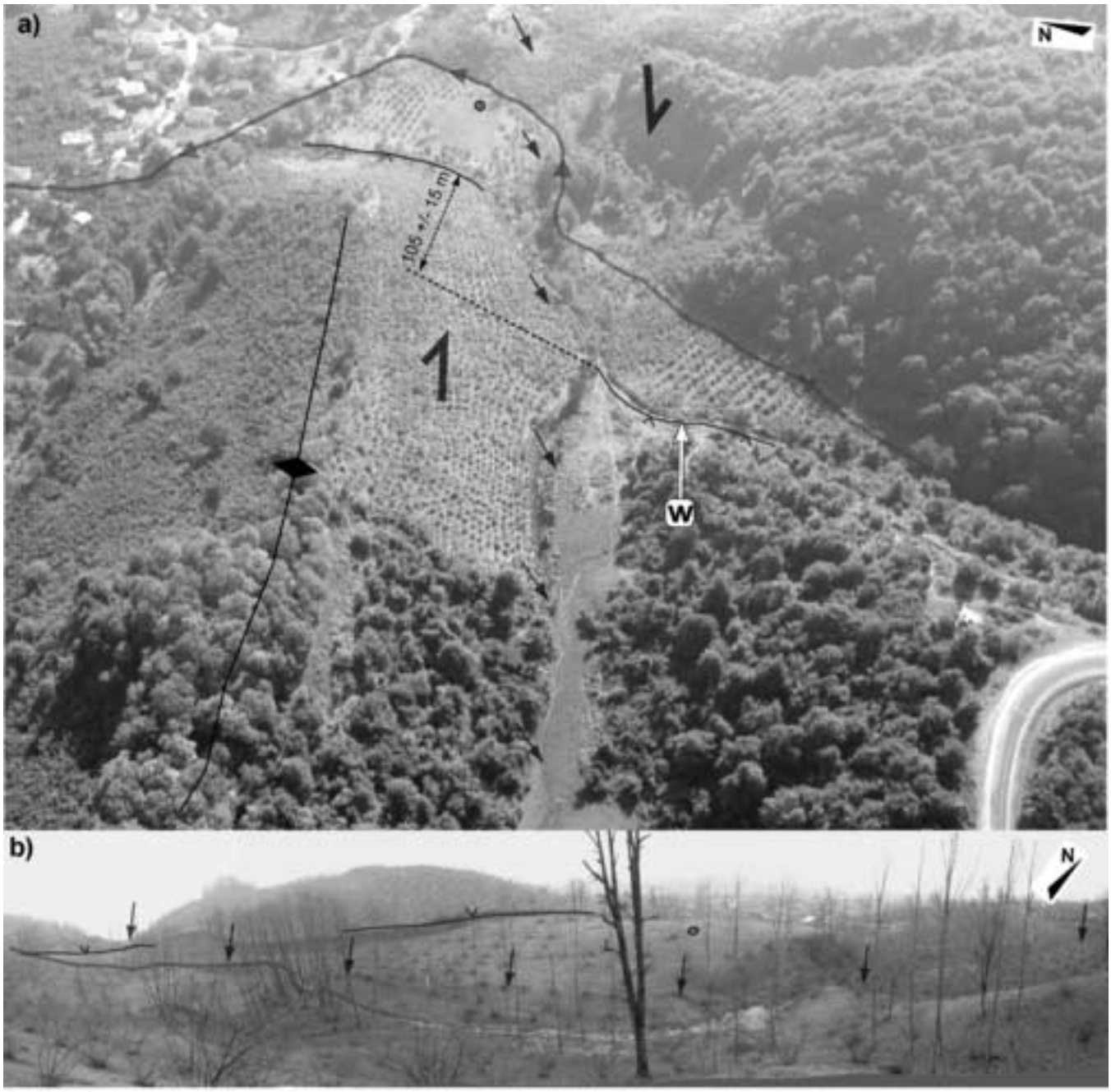

Fig. 9

Figure 10

Click here to download high resolution image

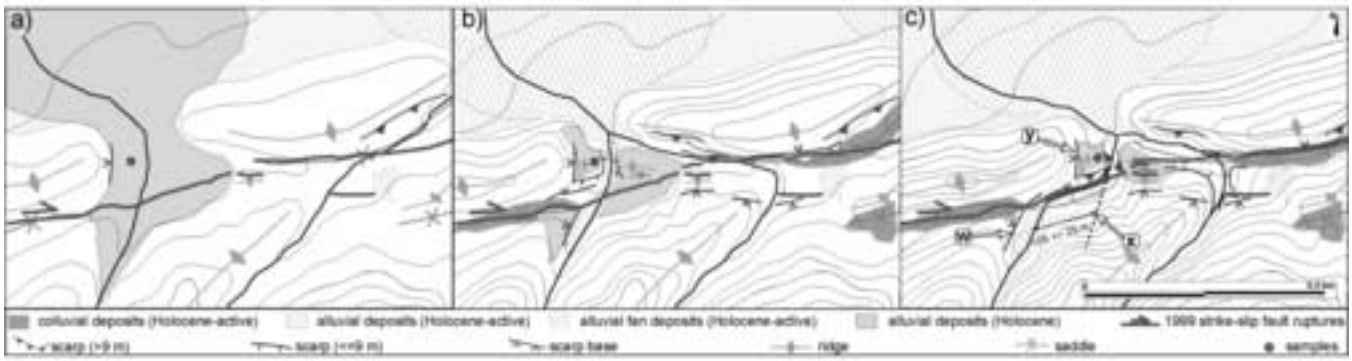

Fig. 10

Figure 11
Click here to download high resolution image

Fig. 11

Figure 12

Click here to download high resolution image

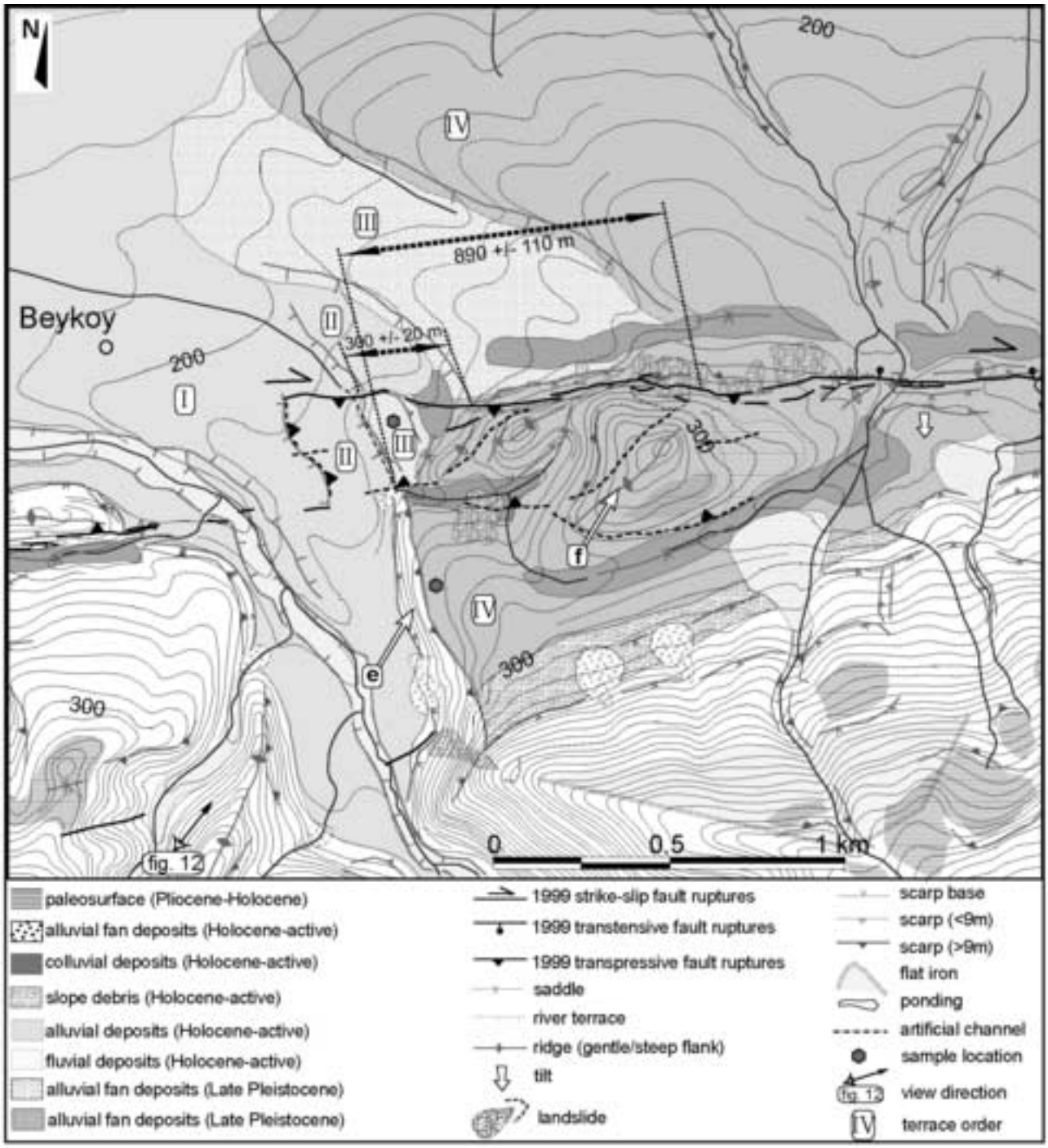

Fig. 12

Figure 13
Click here to download high resolution image

Fig. 13

Figure 14

Click here to download high resolution image

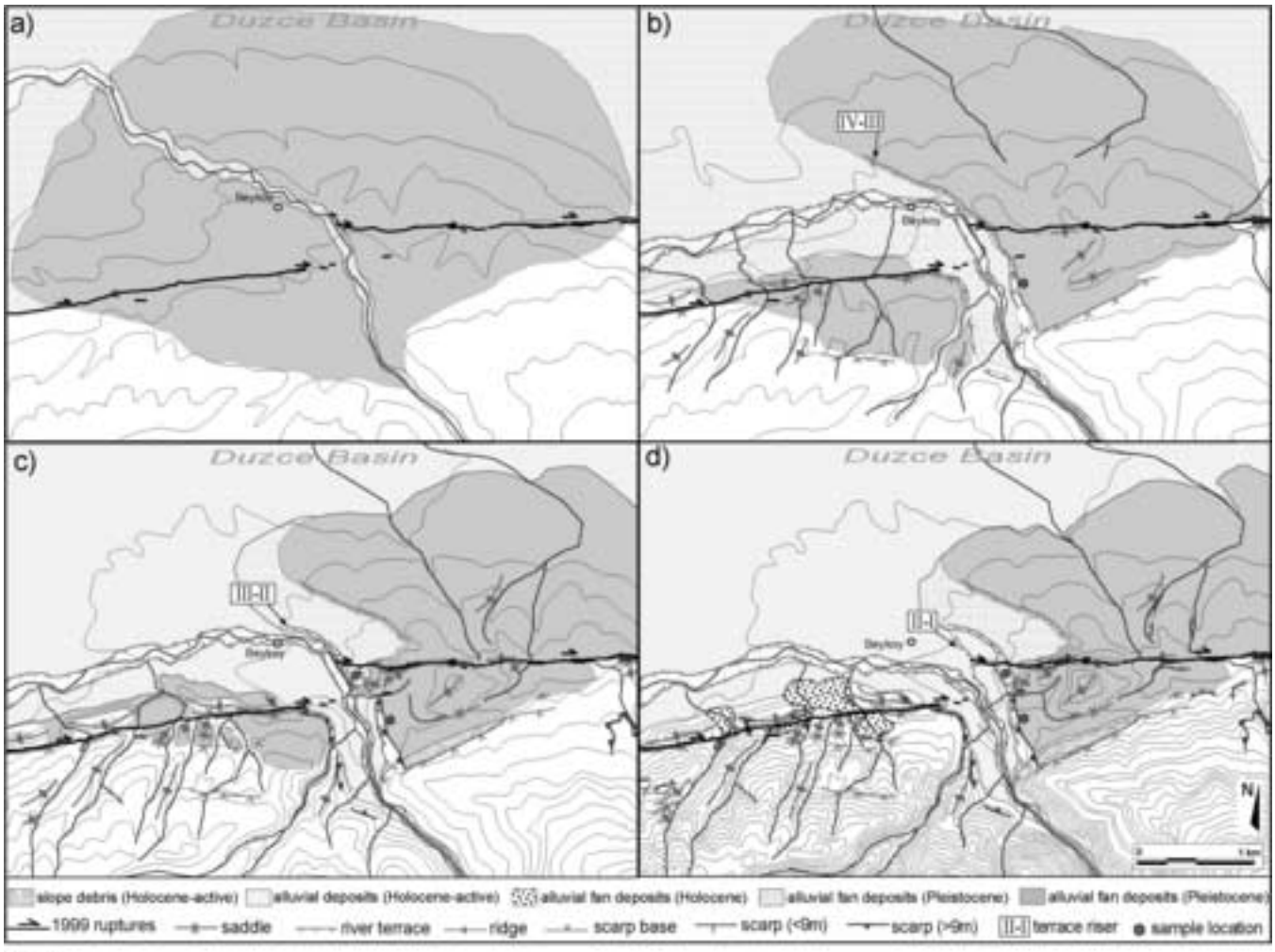

Fig. 14

Figure 15
Click here to download high resolution image

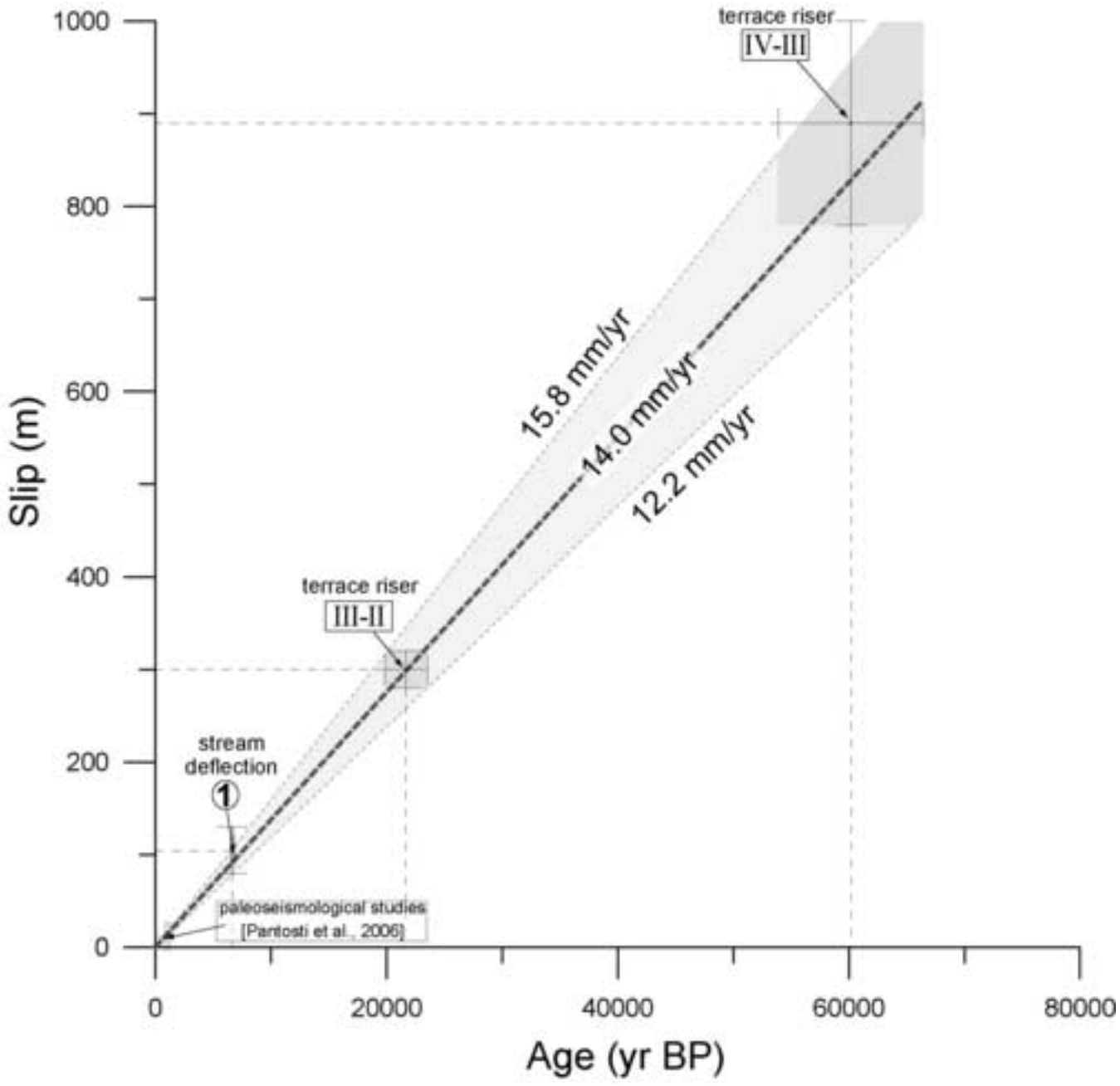

Fig. 15

Table 1

ID	Radiocarbon age (yr BP)	% area enclosed	Cal. AD age ranges (yr BC)	Rel. area under prob. distrib. [Reimer et al., 2004]	Calib. Ages (yr BP)
1	5870 ± 50	68.3 (1σ)	4797 - 4688	1.000	
		95.4 (2σ)	4879 - 4870	0.006	
			4848 - 4595	0.994	6720 ± 120
2	4150 ± 35	68.3 (1σ)	2869- 2835	0.216	
			2816- 2802	0.082	
			2778- 2667	0.701	
		95.4 (2σ)	2878- 2622	1.000	4670 ± 60

Table 1.

Table 2

ID	Equivalent dose (Grays) [a)]	Thermal stability ratio [b)]	A value [c)]	Uranium (ppm) [d)]	Thorium (ppm) [d)]	K20 (%) [d)]	Moisture content (%)	Total dose rate (Grays/ka) [e)]	OSL age (yr BP) [f)]
3	167.02 ± 0.70	1.06 ± 0.03	0.060 ± 0.002	2.01 ± 0.44	9.08 ± 1.25	1.53 ± 0.02	25 ± 5	2.78 ± 0.13	60 170 ± 6280
4	76.04 ± 0.28	0.94 ± 0.03	0.069 ± 0.002	1.46 ± 0.42	9.26 ± 1.23	1.93 ± 0.02	10 ± 3	3.50 ± 0.16	21 700 ± 1850

Table 2.